On the predominance of unstable atmospheric conditions in the marine boundary layer offshore of the U.S. northeastern coast

AGU PUBLICATIONS

JGR

Journal of Geophysical Research: Atmospheres

RESEARCH ARTICLE
10.1002/2016JD024896

Key Points:
- The marine boundary layer offshore of the northeastern U.S. is predominantly unstable
- Nonlogarithmic wind speed profiles are a valid proxy for unstable offshore conditions
- Stable conditions offshore of the northeastern U.S. occur mostly in spring and with southwesterly flow

Correspondence to:
C. L. Archer,
carcher@udel.edu

Citation:
Archer, C. L., B. A. Colle, D. L. Veron, F. Veron, and M. J. Sienkiewicz (2016), On the predominance of unstable atmospheric conditions in the marine boundary layer offshore of the U.S. northeastern coast, *J. Geophys. Res. Atmos.*, *121*, 8869–8885, doi:10.1002/2016JD024896.

Received 3 FEB 2016
Accepted 15 JUL 2016
Accepted article online 18 JUL 2016
Published online 9 AUG 2016

On the predominance of unstable atmospheric conditions in the marine boundary layer offshore of the U.S. northeastern coast

Cristina L. Archer[1], Brian A. Colle[2], Dana L. Veron[1], Fabrice Veron[1], and Matthew J. Sienkiewicz[2]

[1]College of Earth, Ocean, and Environment, University of Delaware, Newark, Delaware, USA, [2]School of Marine and Atmospheric Sciences, State University of New York at Stony Brook, Stony Brook, New York, USA

Abstract The marine boundary layer of the northeastern U.S. is studied with focus on wind speed, atmospheric stability, and turbulent kinetic energy (TKE), the three most relevant properties in the context of offshore wind power development. Two long-term observational data sets are analyzed. The first one consists of multilevel meteorological variables measured up to 60 m during 2003–2011 at the offshore Cape Wind tower, located near the center of the Nantucket Sound. The second data set comes from the 2013–2014 IMPOWR campaign (Improving the Modeling and Prediction of Offshore Wind Resources), in which wind and wave data were collected with new instruments on the Cape Wind platform, in addition to meteorological data measured during 19 flight missions offshore of New York, Connecticut, Rhode Island, and Massachusetts. It is found that, in this region: (1) the offshore wind resource is remarkable, with monthly average wind speeds at 60 m exceeding 7 m s^{-1} all year round, highest winds in winter (10.1 m s^{-1}) and lowest in summer (7.1 m s^{-1}), and a distinct diurnal modulation, especially in summer; (2) the marine boundary layer is predominantly unstable (61% unstable vs. 21% neutral vs. 18% stable), meaning that mixing is strong, heat fluxes are positive, and the wind speed profile is often nonlogarithmic (~40% of the time); and (3) the shape of the wind speed profile (log versus nonlog) is an effective qualitative proxy for atmospheric stability, whereas TKE alone is not.

1. Introduction

Broadly speaking, atmospheric stability is a measure of the potential for vertical motion in the atmosphere. An atmospheric layer is considered stable when it is stratified, vertical motion is suppressed, and the air is cooled from the bottom up (i.e., the surface heat flux is negative, like at night over land). Conversely, in an unstable layer vertical motion is enhanced (upward or downward), the air is heated from the bottom up (i.e., the surface heat flux is positive, like in the daytime over land), and the layer is mixed or overturned by eddies. Lastly, a layer is neutral when it is adiabatic (i.e., with no net heat exchanges), vertical motion is neither enhanced nor suppressed, and no convection is present [*Stull*, 1988]. Static stability is the most commonly used measure of atmospheric stability that is not dependent on wind. The atmosphere is defined as statically stable, unstable, or neutral when the vertical gradient of potential temperature (or virtual potential temperature when moisture is nonnegligible) is positive, negative, or zero, respectively [*Arya*, 1988; *Jacobson*, 2005]. However, static stability is not sufficient to characterize atmospheric stability properly, especially in convective mixed layers and in the presence of shear-generated turbulence [*Stull*, 1988]. Dynamic (i.e., related to wind) information is needed in such cases, in the form of wind shear or turbulent heat and momentum fluxes. The most used parameters are the Richardson number (*Ri*) and the Obukhov length (*L*), both of which include static and dynamic terms like turbulent kinetic energy (TKE) production through buoyancy and shear [*Stull*, 1988]. More details on methods to measure atmospheric stability are presented in section 3.

In the context of wind power, atmospheric stability is important because it impacts the vertical distribution of momentum (e.g., wind shear) and other thermodynamic variables in the atmospheric boundary layer (ABL) and thus affects hub height wind speed, which ultimately determines wind power production. In addition, different stability conditions (stable, unstable, or neutral) are associated with variations in magnitude and distribution of turbulence intensity, thus leading to stresses and fatigue loads on the wind turbines [*Eggers et al.*, 2003; *Guo et al.*, 2015]. Lastly, under stable conditions low-level jets can form close to the hub height of wind turbines and cause extreme, damaging loads on the wind turbines [*Banta et al.*, 2008; *Nunalee and Basu*, 2013]. If numerical weather prediction models are used for wind power forecasts, or for long-term wind resource assessment, or for wind trend analyses, then properly capturing the atmospheric stability conditions is paramount.

At inland wind farms, wind shear and turbulence intensity, which are the two most relevant properties affected by atmospheric stability, have been studied extensively [*Eggers et al*., 2003; *Wagner et al*., 2009; *Antoniou et al*., 2010], but the effect of atmospheric stability, which encompasses both wind shear and turbulence, on wind power generation is still a relatively new topic [*Sumner and Masson*, 2006; *van den Berg*, 2008], with contradictory net impacts. For example, *Wharton and Lundquist* [2012a, 2012b] found that up to 15% more power is generated under stable than unstable conditions for the same hub height wind speed at an inland West Coast North American wind farm, while *Vanderwende and Lundquist* [2012] found instead higher power production during unstable rather than stable conditions at a wind farm located in the High Plains of central North America.

More studies have been published about stability conditions at offshore research sites or offshore wind farms than inland, but only in Europe [*Van Wijk et al*., 1990; *Barthelmie*, 1999; *Lange et al*., 2004; *Barthelmie et al*., 2005; *Sathe et al*., 2011]. *Motta et al*. [2005] showed that neutral stability, an assumption often used in the absence of stability data [*International Electrotechnical Commission*, 2009], is not necessarily the dominant condition at offshore wind sites in Denmark. They introduced revised stability corrections to the conventional logarithmic profile to better estimate the vertical distribution of wind speed. Similarly, *Kettle* [2014] found that nonlogarithmic wind speed profiles, defined as nonmonotonic vertical wind speed profiles with one or more inflection points, are common (~75% of the cases) at the FINO1 offshore research platform in the southern North Sea. Atmospheric stability also impacts wake recovery and wind speed/power deficit; higher deficits were found to be often associated with stable conditions at the Horns Rev offshore wind farm [*Hansen et al*., 2012]. The offshore boundary layer is further complicated by the presence of waves (via the so-called "wave pumping" mechanism) and other horizontal heterogeneities [*Sullivan et al*., 2014; *Hara and Sullivan*, 2015; *Mironov and Sullivan*, 2015], which generally contribute to increased surface roughness, enhanced turbulence, and reduced mean wind shear, even in a statically stable ABL.

Although there are not yet offshore wind farms in the U.S. waters, several are scheduled for installation along the East Coast starting in 2016 (Maryland: https://www.doi.gov/news/pressreleases/interior-auctions-80000-acres-offshore-maryland-for-wind-energy-development-advances-presidents-climate-action-plan, New Jersey: https://www.doi.gov/pressreleases/interior-department-auctions-344000-acres-offshore-new-jersey-wind-energy-development, Block Island (RI): http://www.nytimes.com/2015/07/24/business/offshore-wind-farm-raises-hopes-of-us-clean-energy-backers.html?_r=0, and Massachusetts: http://www.boem.gov/Commercial-Wind-Leasing-Offshore-Massachusetts/). Yet there is no published long-term study on atmospheric stability in the marine boundary layer offshore of the U.S., only two short-term field campaigns. CBLAST (Coupled Boundary Layers/Air-Sea Transfer) investigated air-sea interactions during a few weeks in the summers of 2002 and 2003 using radiosondes, sodar, and a turbulence flux package [*Edson et al*., 2007; *Helmis et al*., 2013, 2015]. POWER (Position of Offshore Wind Energy Resources) was conducted on a cruise along the coast of New England during July–August 2004 and used a high-resolution Doppler lidar to measure wind profiles aloft in the wind turbine rotor area [*Pichugina et al*., 2012].

This study is the first to provide a complete stability analysis at a proposed offshore site along the U.S. East Coast, based on two long-term observational data sets that were collected in the Nantucket Sound. The first data set consists of continuous, multilevel wind observations from a 60 m meteorological mast, near the planned site of the Cape Wind (CW) offshore wind farm. Covering approximately 9 years between 2003 and 2011, this will be referred to hereafter as the "historical data set." The second was collected during the recent, 2 year IMPOWR (Improving the Modeling and Prediction of Offshore Wind Power Resources) campaign [*Colle et al*., 2016] and will be referred to hereafter as the "IMPOWR data set." The IMPOWR campaign was designed to improve our understanding of the marine layer for offshore wind resource assessment.

Given that atmospheric stability has such an important potential impact on the wind resource, the goal of this paper is to provide climatological information on links between stability and wind profiles.

2. Data

2.1. Historical Data at the Cape Wind Meteorological Tower

The Cape Wind (CW) meteorological tower was installed at Horseshoe Shoal in Nantucket Sound in 2002 (Figure 1). The tower has a tripod base with a triangular platform at 10 m above mean lower low water

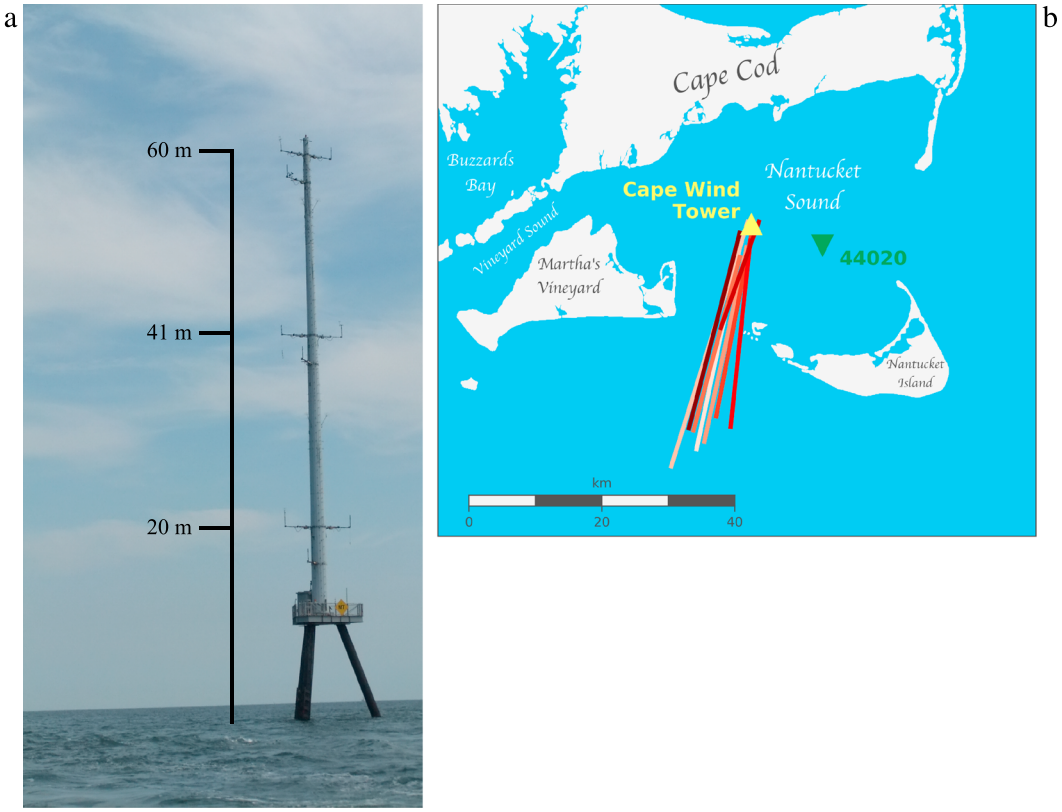

Figure 1. (a) Photo of the Cape Wind meteorological tower (photo credit: D. Veron), showing the three booms with dual wind measurements (cups and sonic anemometers) at 20, 41, and 60 m MLLW, and (b) map showing the location of Nantucket Sound, the Cape Wind tower, buoy 44020, and the eight flight paths of constant altitude discussed later in sections 2.2 and 4.3, with different colors for clarity.

(MLLW) level and instrument arms at 20, 41, and 60 m above MLLW (MLLW omitted hereafter). Wind speed and direction were measured at the three levels using a sonic anemometer paired with a cup anemometer and a wind vane mounted on 9 m booms at each level. Temperature and pressure were measured by paired platinum temperature probes and electronic barometers at 10 and 58.5 m mounted on 1 m booms. The instruments at 10 m were mounted to the side of the platform (Table 1).

Table 1. Details of the Instrumentation Installed on the Cape Wind Meteorological Tower in Nantucket Sound in the Historical and IMPOWR Data Sets

Instrument Type	Data	Accuracy	Height (m Above MLLW)	Orientation From True North (deg)	Data Availability
		Historical Data Set			
Ultrasonic anemometer (RMYoung 8100)	Wind speed Wind direction	±0.05 m s^{-1} ±2°	20, 41, 60	355, 355, 170	20 and 41 m: 9/2003–9/2009 and 60 m: 9/2003–10/2007
Cup anemometer (MetOne 010C)	Wind speed	±0.07 m s^{-1}	20, 41, 60	175, 175, 350	4/2003–9/2009
Vane anemometer (MetOne 023A)	Wind direction	±3°	16.5, 36.5, 55.5	310, 310, 325	20 and 41 m: 4/2003–9/2009 and 60 m: 4/2003–4/2008
Temperature sensor (RMYoung 4134VC)	Air temperature	±0.3°C	10, 58.5	210, 170	5/2003–9/2009
Pressure sensor (RMYoung 61202)	Air pressure	±1 hPa	10, 58.5	210, 170	5/2003–9/2009
		IMPOWR Campaign			
Ultrasonic anemometer (RMYoung 8100)	Wind speed Wind direction	±0.05 m s^{-1} ±2°	12	210, 330	3/2013–5/2013, 8/2013, 10/2013–6/2014
Temperature probe (RMYoung 41342LC)	Air temperature	±0.3°C	11	210	3/2013–5/2013, 8/2013, 10/2013–6/2014
Temperature and relative humidity probe (RMYoung 41382LC)	Air temperature and relative humidity	±0.3°C and ±2%	11	330	3/2013–5/2013, 8/2013, 10/2013–6/2014
Optical wave gauge (ILM150)	Wave height	±0.5 cm	11	200	3/2013–5/2013, 8/2013, 10/2013–6/2014

Table 2. Details of the Eight Flights During IMPOWR That Maintained a Relatively Constant Altitude Below 90 m for at Least 5 min[a]

Date (yyyymmdd)	Start (HHMM, UTC)	Stop (HHMM, UTC)	Distance (km)	Heading (deg)	Altitude (m)	Wind Speed ($m\,s^{-1}$)	Wind Direction (deg)	TKE ($m^2\,s^{-2}$)
20130404	2003	2008	17	200	70	11	230	0.55
20130504	2051	2058	30	190	90	12	50	0.81
20130510	1918	1926	32	190	30	7	200	0.67
20130620	1752	1758	28	10	40	9	220	0.82
20130621	1853	1900	33	10	40	10	220	1.49
20130623	2121	2131	38	200	30	12	160	2.03
20130928	2003	2010	30	10	30	5	80	1.33
20131002	1852	1859	27	190	30	8	250	1.42

[a]The values are averages over the flight leg.

The meteorological instrumentation started recording observations in April 2003 and continued until August 2011, with data sampled at 1 Hz and then averaged and archived every 10 min. Factory calibration coefficients were applied before averaging. The primary purpose of the CW tower was to characterize the wind resource for the proposed Cape Wind Energy Project, a 468 MW project (http://www.boem.gov/Renewable-Energy-Program/Studies/Cape-Wind.aspx). The anemometers were regularly maintained and calibrated through 2007, with continuous recordings at all levels. After 2007, the instruments were left in continual operation but they were not maintained or calibrated, as the archived data were sufficient for wind resource characterization. Eventually, several of the instruments failed (e.g., the 60 m sonic anemometer in late 2007), while some remained in operation through 2011. We had access to the original 10 min data from the data logger. We do not analyze data beyond 2009, 2 years after the final instrument calibration (Table 1).

The raw wind data from the CW tower are processed at each level following three steps. First, wind speed ($0\,m\,s^{-1} \le U \le 30\,m\,s^{-1}$) and direction filters ($0° \le \phi < 360°$) are applied to remove nonphysical values. The wind speeds were limited at $30\,m\,s^{-1}$ to focus on situations when typical offshore wind turbines would be in operation; this limits our analysis to moderate wind speeds. Second, any nonphysical changes in wind speed and direction are also removed, such as large jumps in wind speed and direction (e.g., more than doubling of the wind speed in 10 min for wind speeds $>3\,m\,s^{-1}$) or significant discrepancies between the sonic anemometer and the cup anemometer or wind vane (e.g., >15° direction difference or 30% wind speed ratio). Third, as can be seen in Figure 1a, the presence of the monopile influences the wind observations, creating directional sectors where the observations are not valid. The sonic anemometer, wind vane, and cup anemometer were installed on separate booms at different angles to assist with this problem (Table 1). Data are removed from analysis when the monopile is directly upstream of a wind sensor (±30°), following *Brower* [2012]. Therefore, at each level the wind speed and direction are taken from the instrument that is unhindered by the presence of the monopile; if both instruments have good data (i.e., not downwind of the monopile), then the observations are averaged together; if neither instrument has good data, then the data are removed.

2.2. The IMPOWR Field Campaign

The IMPOWR (Improving the Mapping and Prediction of Offshore Wind Resources) field study was conducted in the Nantucket Sound area in 2013–2014. The IMPOWR campaign provided observations within the ABL from a Long-EZ aircraft, along with oceanic and atmospheric measurements on the Cape Wind tower, and lidars on the south shore of eastern Long Island and Block Island [*Colle et al.*, 2016].

A Long-EZ aircraft was used during 2013, while a Cozy Mark IV aircraft was used after the fall of 2014. Both aircrafts carried the Aircraft-Integrated Meteorological Measurement System (AIMMS-20) instrument in order to measure the three-dimensional winds, temperature, pressure, and relative humidity at 40 Hz. Nineteen flight missions originated from Brookhaven Airport; this study focuses only on eight missions (Figure 1b and Table 2), during which a constant flight altitude below 90 m was maintained for over 5 min, a length of time comparable to the averaging interval used in the historical data set.

In March 2013, two sonic anemometers, a temperature probe, a temperature and relative humidity probe with aspirated shield, and a high-speed optical wave gauge were installed along two sides at about 2 m above the platform of the CW tower (Table 1). The data were recorded continuously at 20 Hz and transmitted from the tower every 10 min; they were archived in both averaged and raw form. Prior to averaging, the data

were despiked using an algorithm based on *Goring and Nikora* [2002]. The data were also rotated to account for small mounting misalignments [*Wilczak et al.*, 2001]. The data were systematically removed if $u_* > 10\,\mathrm{m\,s^{-1}}$, if the standard deviation of any wind speed component exceeded $10\,\mathrm{m\,s^{-1}}$, and for data leading to a drag coefficient $C_d > 0.01$ [*Foken et al.*, 2004].

The data taken when an instrument was in the wake of the tower were removed based on wind directions from nearby buoy 44020 (Figure 1b). When this occurred, a 90° sector was eliminated to account for the large wake of the tower platform at this height. If both sonic anemometers had wind speeds that passed the above quality control criteria, then they were averaged together. During the winter months the system had to run a 6 h reduced power cycle because of limited energy storage in the solar batteries. Also, no data were transmitted during July 2013 and July 2014 because of a loss in connectivity.

During the IMPOWR campaign, no winds in excess of $30\,\mathrm{m\,s^{-1}}$ were observed at the tower or at buoy 44020.

3. Methods to Characterize Atmospheric Stability

Atmospheric stability is often determined by static considerations alone using the vertical gradient of potential temperature $\left(\frac{\partial\theta}{\partial z}\right)$ or virtual potential temperature $\left(\frac{\partial\theta_v}{\partial z}\right)$ in dry and moist conditions, respectively, and thresholds to separate stable, unstable, and neutral conditions. This approach completely neglects the dynamic effect of wind, thus providing an incomplete picture of mixing in the atmosphere. Additionally, in a marine environment such as Nantucket Sound, specific humidity is high and therefore virtual potential temperature, not just potential temperature, should be used for determining static stability [*Arya*, 1988; *Stull*, 1988]. Unfortunately, humidity measurements were not available at the CW tower in 2003–2009 and therefore neither virtual temperature nor its vertical gradient could be calculated. This study proposes three alternative parameters to characterize atmospheric stability in the marine ABL, namely, the Obukhov length, the shape of the wind speed profile, and turbulent kinetic energy, as described next.

3.1. The Obukhov Length

The Obukhov length L, first identified by Obukhov in 1946 [*Obukhov*, 1946], is often referred to as the Monin-Obukhov length because it was used extensively later in 1954 in the similarity theory by both Monin and Obukhov [*Arya*, 1988]. The Obukhov length represents the lowest height above the ground at which TKE production by buoyancy dominates over that by mechanical effects, such as shear and friction. Intuitively, L is infinite in a neutral atmosphere because buoyancy is absent by definition. Conversely, in both stable and unstable conditions, buoyancy is the driving force and therefore the magnitude of L is small, indicating that shear and friction are important only close to the surface.

Whereas the meaning of L is clear, its formulation varies depending on the type of measurements available and on the level of moisture in the atmosphere. In a dry atmosphere characterized by surface heat flux H_0 (positive upward and negative downward), friction velocity u_*, and near-surface temperature T_0, L is defined as

$$L = -\frac{u_*^3}{k\frac{g}{T_0}\frac{H_0}{\rho c_p}}, \tag{1}$$

where k is the von Karman constant (~0.4), ρ the air density, and c_p the air specific heat. The minus sign defines L to be negative for unstable conditions, when the heat flux is positive and upward, and positive for stable conditions [*Arya*, 1988].

If moisture is high, like often in the marine ABL, then the buoyancy effect of water vapor must be taken into account by replacing temperature and heat flux in equation (1) with virtual temperature and virtual heat flux [*Arya*, 1988; *Stull*, 1988; *Arya*, 1999]. Since a sonic anemometer measures a value of air temperature T_s that is very close to virtual temperature T_v in the presence of water vapor [*Schotanus et al.*, 1983; *Kaimal and Gaynor*, 1991; *Wyngaard*, 2010], the definition of L adopted here is

$$L = -\frac{u_*^3}{k\frac{g}{T_v}\overline{w'T_v'}} \sim -\frac{u_*^3}{k\frac{g}{T_s}\overline{w'T_s'}}, \tag{2}$$

where $\overline{w'T_v'}$ is the virtual heat flux, $\overline{w'T_s'}$ is the sonic heat flux (a proxy for $\overline{w'T_v'}$), T_s is measured at the height of the sonic anemometer, and u_* is calculated at the height of the sonic anemometer. The Reynolds averaging convention is used here, by which a prime $(\cdot)'$ indicates a turbulent component and a bar $\overline{(\cdot)}$ a time average.

Table 3. Ranges of Obukhov Length L Used in the Literature and in This Study[a]

Study	Very Unstable	Unstable	Neutral	Stable	Very Stable	Notes
Van Wijk et al. [1990]	$-200 < L < 0$	$-1000 < L < -200$	$\|L\| > 1000$	$200 < L < 1000$	$0 < L < 200$	Offshore, three sites
Motta et al. [2005]	$-200 < L < 0$	$-1000 < L < -200$	$\|L\| > 1000$	$200 < L < 1000$	$0 < L < 200$	Offshore, four sites; air temperature and wind sensors at various heights
Gryning et al. [2007]	$-100 < L < -50$	$-500 < L < -100$	$\|L\| > 500$	$50 < L < 500$	$10 < L < 50$	Inland; 10 or 50 m sonics
Sathe et al. [2011]	$-100 < L < -50$	$-500 < L < -100$	$\|L\| > 500$	$50 < L < 500$	$10 < L < 50$	Offshore; air and seawater temperature at 21 and -3.8 m or 13 and -4 m; wind at 21 m or 15 m
Högström [1988]		$\zeta < -0.1$	$-0.1 < \zeta < 0.1$	$\zeta > 0.1$		Inland; hot-wire anemometers at 3, 6, and 14 m
Metzger et al. [2007]		$\zeta < -0.1$	$-0.1 < \zeta < 0.1$ ($\|L\| > 200$)	$\zeta > 0.1$		Inland; nine sonics at 1.4–26 m; assumption $T_v = T_s$.
Rajewski et al. [2013]		$\zeta < -0.05$	$-0.05 < \zeta < 0.05$ ($\|L\| > 400$)	$\zeta > 0.05$		Inland; sonics at 4.5 or 6.5 m; uncorrected flux using $T = T_v = T_S$.
Wharton and Lundquist [2012a, 2012b]	$-50 < L < 0$	$-600 < L < -50$	$\|L\| > 600$	$100 < L < 600$	$0 < L < 100$	Inland; 3 m sonic; SODAR and cup at 80 m
This study	$-100 < L < -5$	$-500 < L < -100$	$\|L\| > 500$	$100 < L < 500$	$5 < L < 100$	Offshore; 20 m sonics

[a]All ranges are in units of meters (m). If only ζ was provided in the original study, the expected value of L at CW is reported in parentheses.

The sonic anemometer located at $z_s = 20$ m on the CW tower was used to calculate L because it was the closest to the water and had the longest record. From the 20 m horizontal wind speed $U(20)$, u_* is obtained as follows:

$$u_* = \frac{kU(20)}{\log\left(\frac{20}{z_0}\right) - \Psi_m}, \tag{3}$$

where z_0 is the (dynamic) surface roughness. Ψ_m is the stability function, which depends on L:

$$\Psi_m = \begin{cases} 2\ln\frac{1+x}{2} + \ln\frac{1+x^2}{2} - 2\tan^{-1}x + \frac{\pi}{2} & L < 0 \\ 0 & L \to \infty \\ -5\frac{z_s}{L} & L > 0, \end{cases} \tag{4}$$

where $x = \left(1 - \frac{z_s}{L}\right)^{1/4}$. Since there are three unknowns (z_0, L, and u_*), but only two equations (2) and (3), an iterative method is used [*Van Wijk et al.*, 1990; *Motta et al.*, 2005] to obtain estimates of L from the historical data set with a time resolution of 10 min. Note that, when the atmosphere is neutral, Ψ_m is zero and equation (4) reduces to the log law:

$$U(z) = u^*/k \log(z/z_0) \tag{5}$$

The next challenge in classifying the atmospheric stability at CW is the definition of the Obukhov length thresholds for stable, neutral, and unstable conditions. A broad range of thresholds has been used in previous studies (Table 3). For example, *Motta et al.* [2005] studied four offshore wind farms in the North Sea, most of which had measurement heights similar to the CW tower. They used the largest threshold to identify neutral conditions (i.e., $|L| > 1000$ m), based on *van Wijk et al.* [1990], and included limits for "very stable" and "very unstable" conditions. *Sathe et al.* [2011] used a lower threshold for neutral stability ($|L| > 500$ m), nonsymmetric ranges for stable versus unstable conditions, following *Gryning et al.* [2007], and seawater temperature in their calculation of L. *Rajewski et al.* [2013] conducted two intense field campaigns at an inland wind farm in Iowa and did not use L but rather $\zeta = \frac{z}{L}$, with z being the height of the sonic (4.5 or 6.5 m), to categorize stability. They chose a threshold of $|\zeta| <= 0.05$ for near-neutral conditions, which means that the value of L associated with neutrality was 90–130 m, the smallest value found in the literature. All other studies used a higher value of ζ (i.e., $|\zeta| > 0.1$) for neutral stability [*Högström*, 1988; *Metzger et al.*, 2007], corresponding to $|L| > 200$ m at CW.

The ranges of L used in this study, shown in Table 3, are a blend of those found in the literature and have desirable properties, such as an average virtual heat flux that is over 5 times greater in unstable (0.047 K m s^{-1})

than in neutral (0.008 K m s^{-1}) conditions and ~50% stronger in stable ($|-0.012|$ K m s^{-1}) than in neutral conditions [*Metzger et al.*, 2007].

3.2. Shape of the Wind Speed Profile

The primary method to determine atmospheric stability at CW employs the Obukhov length, because it includes both buoyancy and mechanical effects and because virtual temperature fluxes were available from the sonic anemometers. However, this method assumes a logarithmic shape of the wind speed profile, which implies that wind speed increases monotonically with height. This is a poor assumption under unstable conditions, where the vertical wind speed profile may be uniform due to strong mixing or even present multiple inflection points [*Kettle*, 2014], possibly due to transient eddies of multiple sizes and durations. As such, a stability analysis based on L alone may not be sufficient because of its numerous underlying assumptions, discussed, for example, in *Arya* [1999], and thus the analysis can benefit from additional evidence provided via more qualitative analyses. A couple of examples are proposed here.

Although wind shear can be driven by large-scale processes, such as advection or pressure gradients, the vertical profile of wind speed in the lower ABL is generally driven by surface heat fluxes. For example, in the presence of negative surface heat fluxes, the ABL becomes increasingly more stable as it cools and wind shear increases, while with positive surface heat fluxes the ABL becomes more unstable as it warms from below and wind shear is low, as shown, for example, in high-resolution numerical simulations (N. S. Ghaisas et al., Evaluation of layout and atmospheric stability effects in wind farms using large-eddy simulation, *Wind Energy*, under review, 2016). Qualitative stability criteria have been developed based on wind shear [*Wharton and Lundquist*, 2012a, 2012b], using the shear exponent α in the so-called power law:

$$\frac{U(z_2)}{U(z_1)} = \left(\frac{z_2}{z_1}\right)^{\alpha}, \tag{6}$$

where $U(z_i)$ is the horizontal wind speed at height z_i ($i = 1,2$). A typical value of α is 1/7 (0.14) for neutral conditions; α generally gets larger as the atmosphere becomes more stable, and it can be negative in strongly unstable conditions [*Wharton and Lundquist*, 2012a, 2012b].

Because the CW tower has three vertical levels (20, 41, and 60 m), three values of α can be calculated, one for each pair of levels. Since these levels are close to each other and close to the ocean surface, there are large discrepancies in the stability classification depending on which α value is selected. Also, the power law is a not an accurate approximation for the logarithmic wind speed profile above the surface layer during unstable conditions [*Emeis*, 2013], which are the most common in the Nantucket Sound, as will be discussed in section 4. Since this method did not produce consistent results, it will not be explored further in this study.

Instead, a simpler approach is proposed here, based on horizontal wind speed values at the three vertical levels, namely, $U(20)$, $U(41)$, and $U(60)$. When wind speed increases monotonically from one level to the next (i.e., $U(60) > U(41) > U(20)$), a logarithmic fit is theoretically possible and therefore the profile is classified as "log"; otherwise, it is classified as "nonlog." This simple algorithm was chosen over more sophisticated methods, such as least square error fits [*Archer and Jacobson*, 2003, 2005] or a priori classifications of zigzag types [*Kettle*, 2014], because of its simplicity and objectivity. However, there are two important limitations. Whereas nonlog profiles are very likely to occur in unstable conditions and very unlikely to occur in stable conditions (as long as low-level jets at very low altitudes are not present, as discussed in section 4.2), log profiles can occur in any stability condition, including unstable. This means that using nonlog profiles alone as a proxy for unstable conditions leads to an underestimation of the frequency of unstable conditions. Second, the classification based on monotonicity alone is useful only when considering the overall statistical distribution but should not be used to explain each individual profile and why it was associated with a certain value of L at a certain time.

3.3. Turbulent Kinetic Energy

Turbulent kinetic energy (TKE) is a measure of the intensity of turbulence in the atmosphere and it is defined as half of the sum of the wind velocity variances:

$$\mathrm{TKE} = \frac{1}{2}\left(\overline{u'^2} + \overline{v'^2} + \overline{w'^2}\right), \tag{7}$$

where u', v', and w' are perturbations around the mean of the west-east, south-north, and vertical wind velocity components. Qualitatively, higher values of TKE indicate stronger turbulence and therefore may

be more common in unstable conditions. However, such a clear relationship between TKE and atmospheric stability is not found in the wind energy literature, where TKE is never adopted alone as a proxy for stability. Rather, TKE ranges are used together with other stability parameters, such as L or α. For example, *Wharton and Lundquist* [2012a, Table 2] propose that, over an inland wind farm, stable conditions are characterized by TKE $< 0.7\,m^2\,s^{-2}$, unstable by TKE > 1.0, and neutral by $0.7 <$ TKE < 1.0 (all values in $m^2\,s^{-2}$), where the measurements are taken at 80 m. However, no such ranges were found in the literature for offshore conditions. Using 4 years of lidar-derived data at an offshore site in Norway, *Christakos et al*. [2013] tried to identify ranges for TKE, without success, and only found one clear relationship between TKE and wind profiles, namely, that "the higher TKE, the higher the wind speed." This suggests that the link between TKE and stability is less straightforward offshore than inland, a conclusion that will also be reached in this study.

Measurements of the variances of the three components of wind velocity were available at a frequency of 10 min from the sonic anemometers at the three levels of the CW tower in the historical data set. The only quality check applied to these data was the removal of horizontal and vertical velocity variances greater than 36 u_*^2 and 16 u_*^2 (thus 36 and 16 $m^2\,s^{-2}$, respectively, assuming a maximum value of u^* equal to 1 $m\,s^{-1}$) [*Panofsky et al*., 1977], or negative, and vertical velocities $>2\,m\,s^{-1}$.

During the IMPOWR campaign, numerous spiraling flights were made around the CW tower to attempt to measure vertical profiles of atmospheric properties, including the three components of wind velocity needed for TKE. However, the aircraft was at a given altitude only for a brief amount of time, on the order of a few seconds. As such, statistical properties that depend on the averaging interval, like TKE, could not be computed reliably because they were too sensitive to the length of the averaging interval [*Vecenaj et al*., 2012]. In addition, since the CW historical TKE data were 10 min averages, comparable averaging intervals for the IMPOWR flights were desirable. Following literature recommendations [*Bond et al*., 2010; *Zhang et al*., 2011], TKE was computed instead over flight legs that were characterized by approximately the same altitude above the ocean for at least 5 min. Out of the 19 missions, eight had these desired altitude and time characteristics, in and out of the Nantucket Bay (Table 2).

4. Results

The historical CW data show that the wind resource along the northeastern U.S. coast is remarkable. The monthly average wind speeds are in excess of 8 $m\,s^{-1}$ for 6 months out of the year even at 20 m (Figure 2a), with highest winds in winter (9.2, 9.8, and 10.1 $m\,s^{-1}$ at 20, 41, and 60 m) and lowest in summer (6.3, 6.7, and 7.1 $m\,s^{-1}$ at 20, 41, and 60 m). Wind speeds are generally higher at higher levels (7.8, 8.4, and 8.8 $m\,s^{-1}$ yearly averages at 20, 41, and 60 m), although exceptions are common, some of which will be described later. Winds from the southwest prevail in summer and from the northwest in winter (Figures 2b and 2c). There is a distinct diurnal pattern (Figures 2d and 2e), especially in summer, when the highest speeds occur in the afternoon around 15 local standard time (LST) (Figure 2e), coinciding with the time of highest electricity demand. This is another reason that this location is highly desirable for offshore wind energy development.

The stability analysis based on the Obukhov length L is accompanied by an analysis of the frequency of logarithmic (log) versus nonlogarithmic (nonlog) wind speed profiles in section 4.1, with the underlying hypothesis, verified in section 4.2, that unstable conditions are more likely to be associated with nonlog profiles, while stable and neutral conditions are more likely to be associated with log profiles. Lastly, additional evidence on the predominance of unstable conditions in Nantucket Sound is provided in section 4.3 via observed TKE statistics during IMPOWR flights.

4.1. Highest Frequency of Unstable Conditions

Unstable conditions generally dominate at the CW tower during the entire historical period (2003–2009), occurring between 40 and 80% of the time depending on the season and time of day (Figure 3). This can be explained in part by the temperature difference between the ocean water and the air. At buoy 44020 (Figure 1b), data from 2009 to 2014 show that the air is generally cooler than the water, by −1.07°C on average, which is conducive to (statically) unstable conditions.

Seasonally (Figure 3a), atmospheric stability is also influenced by the ocean's thermal inertia. In the summer months (June-July-August (JJA)), the air is warmest but the temperature difference between air and water is

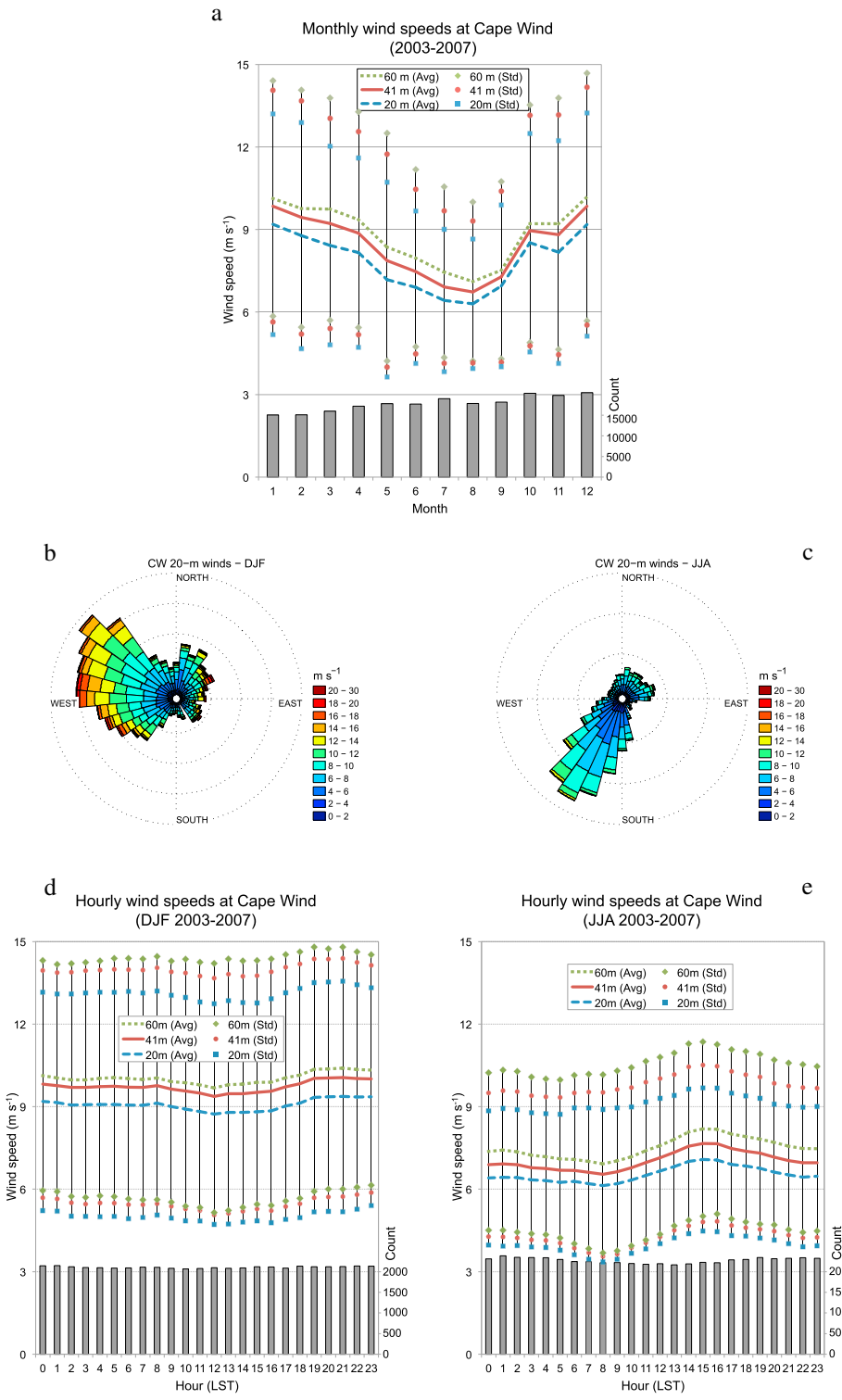

Figure 2. Wind statistics at the Cape Wind tower in 2003–2007: (a) average wind speed by level and by month, wind roses at 20 m in (b) DJF and (c) JJA (reproduced with permission from *Colle et al*. [2016]), and average wind speed by level and by hour in (d) DJF and (e) JJA. In Figures 2a, 2c and 2d, the monthly means ("Avg") are represented with solid or dashed lines, the standard deviations ("Std") with different markers for each level, and the count of valid 10 min records with grey column bars.

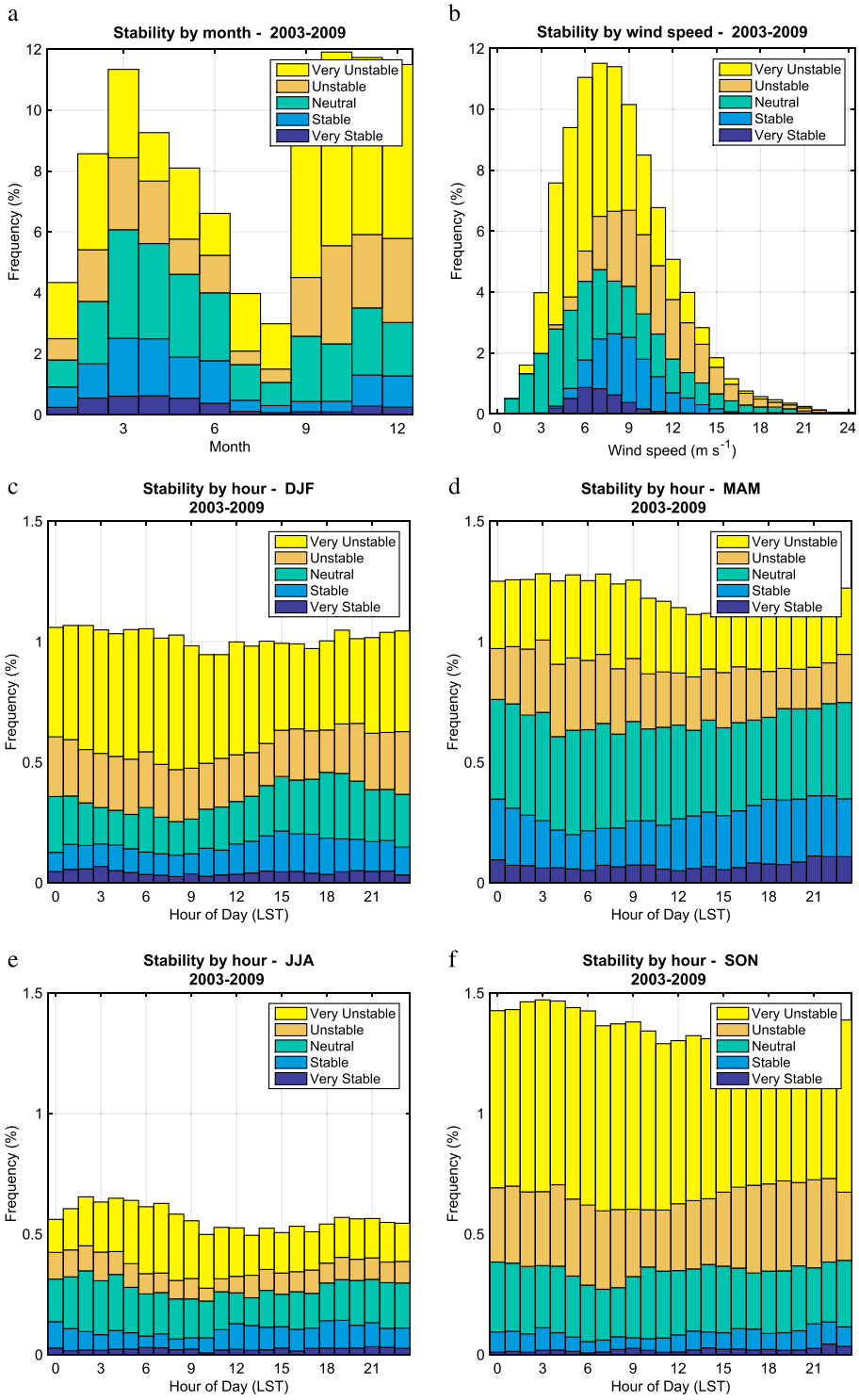

Figure 3. Frequency distributions of atmospheric stability at the Cape Wind tower by (a) month, (b) wind speed bins, and hour of the day in (c) DJF, (d) MAM, (e) JJA, and (f) SON. Frequencies refer to the entire period, not to each season.

lowest in spring (−0.12°C in spring versus −0.70°C in summer); thus, the most frequent stable conditions occur in spring (25%). The strongest temperature difference between water and air occurs in fall and winter (−1.57 and −2.03°C, respectively); thus, fall and winter are the seasons with the highest frequencies of unstable conditions (77% and 63%, respectively), with October having the absolute highest (82%).

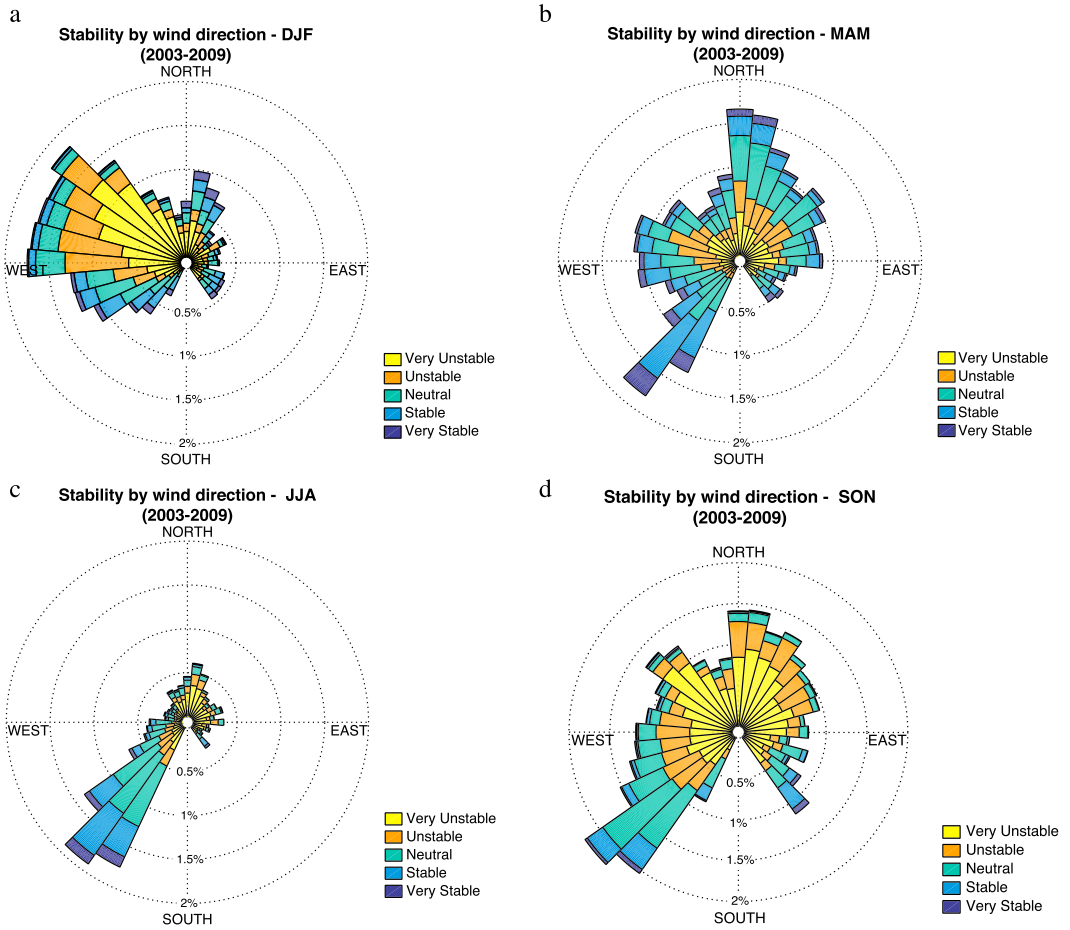

Figure 4. Frequency distribution of atmospheric stability by wind direction at the Cape Wind tower in (a) DJF, (b) MAM, (c) JJA, and (d) SON. Frequencies refer to the entire period (2003–2009), not to each season. Due to the influence of the tower monopile, data in the 150–190° range were discarded.

The wind speed frequency distribution (Figure 3b) indicates that, again, unstable conditions prevail in general. Very stable conditions do not occur at high speeds and are generally infrequent. Neutral conditions are more common at low ($<4\,m\,s^{-1}$) or high ($>18\,m\,s^{-1}$) speeds. Intermediate wind speeds (6–9 $m\,s^{-1}$), perhaps the most relevant for wind energy because they are associated with the highest wake losses, are characterized by the lowest frequency of neutral stability conditions (17–23%), which suggests that the common assumption of neutral stability is not justified, at least in this region.

Diurnally (Figures 3c–3f), the hourly distribution of stability conditions is consistent with the seasonal one discussed above, with the highest frequency of stable and unstable conditions in spring and fall, respectively. In all seasons, unstable conditions are more likely to occur in the early morning (5–9 LST) and stable conditions in the evening (18–23 LST), which suggests a large role of air advection from the surrounding land.

Atmospheric stability depends strongly on wind direction too (Figure 4), with stable conditions associated almost exclusively with south-southwesterly flow (210–230°), aligned with the gap between the Nantucket and Martha's Vineyard islands. Marine air that comes through this gap has likely developed an internal boundary layer due to warm air advected from the land to the southwest over the cool water. In the warm season (March-April-May (MAM)-JJA, Figures 4b and 4c), this south-southwesterly flow is very common, due to the presence of the Bermuda High, and is accompanied by advection of warm air from the south and thus the highest frequency of stable conditions. Easterly and northeasterly winds, coming from the cooler, open ocean, cause more unstable conditions. Winds from the north and from the northwest in the cold season (September-October-November (SON)-December-January-February (DJF), Figures 4a and 4d)

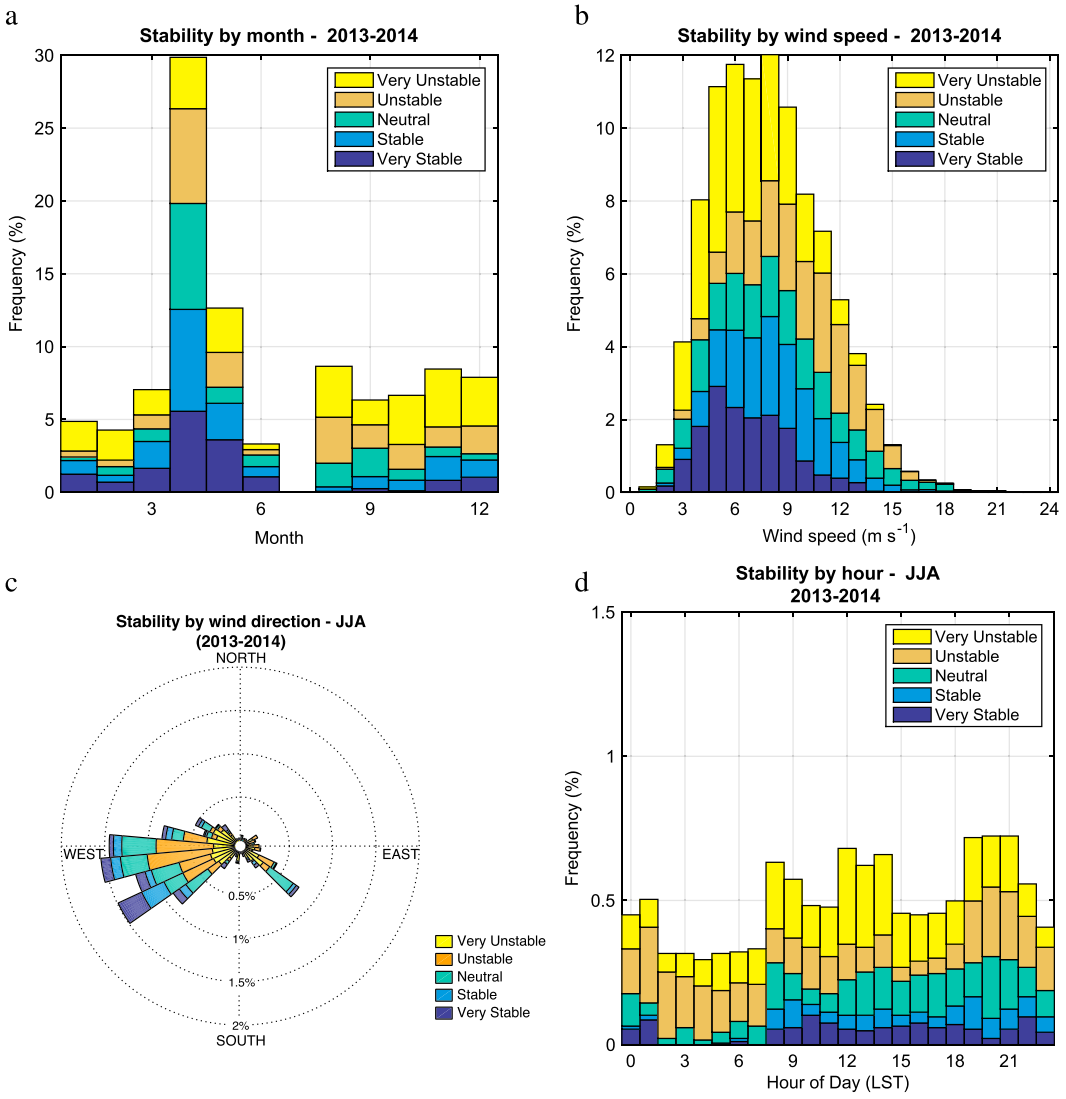

Figure 5. Frequency distributions of atmospheric stability at the Cape Wind tower during the 2013–2014 IMPOWR field campaign: (a) by month, (b) by wind speed, (c) by wind direction in JJA, and (d) by hour in JJA. Due to the irregular data retrieval, more data were collected in April (30%) than any other month.

are associated with the highest frequency of unstable conditions because they have interacted with the cold and rough continental terrain.

IMPOWR data at CW (temperature, virtual heat flux, and wind speed at 10 m) were used to calculate L following the same procedure described in section 3.1. The results are consistent qualitatively with the historical findings (Figure 5). Because of the irregular data retrieval procedure, no data were collected in July of any year and more data were collected in April (30%) than any other month. Since April is generally the most stable month, also from the historical data (Figure 3a), this caused a spurious higher frequency of stable conditions from the IMPOWR than from the historical data (34% versus 15%). Other than that, all other properties are qualitatively similar between the CW historical and IMPOWR data, including the predominance of stable, southwesterly flows in the summer (Figure 5d) and the highest frequency of unstable conditions in October (Figure 5a).

4.2. Nonlogarithmic Wind Speed Profiles as a Proxy for Unstable Conditions

Following the methodology described in section 3.2, the observed historical wind speed profiles at CW were classified as either log or nonlog. The frequency of nonlog events is rather large, ~40%, which suggests

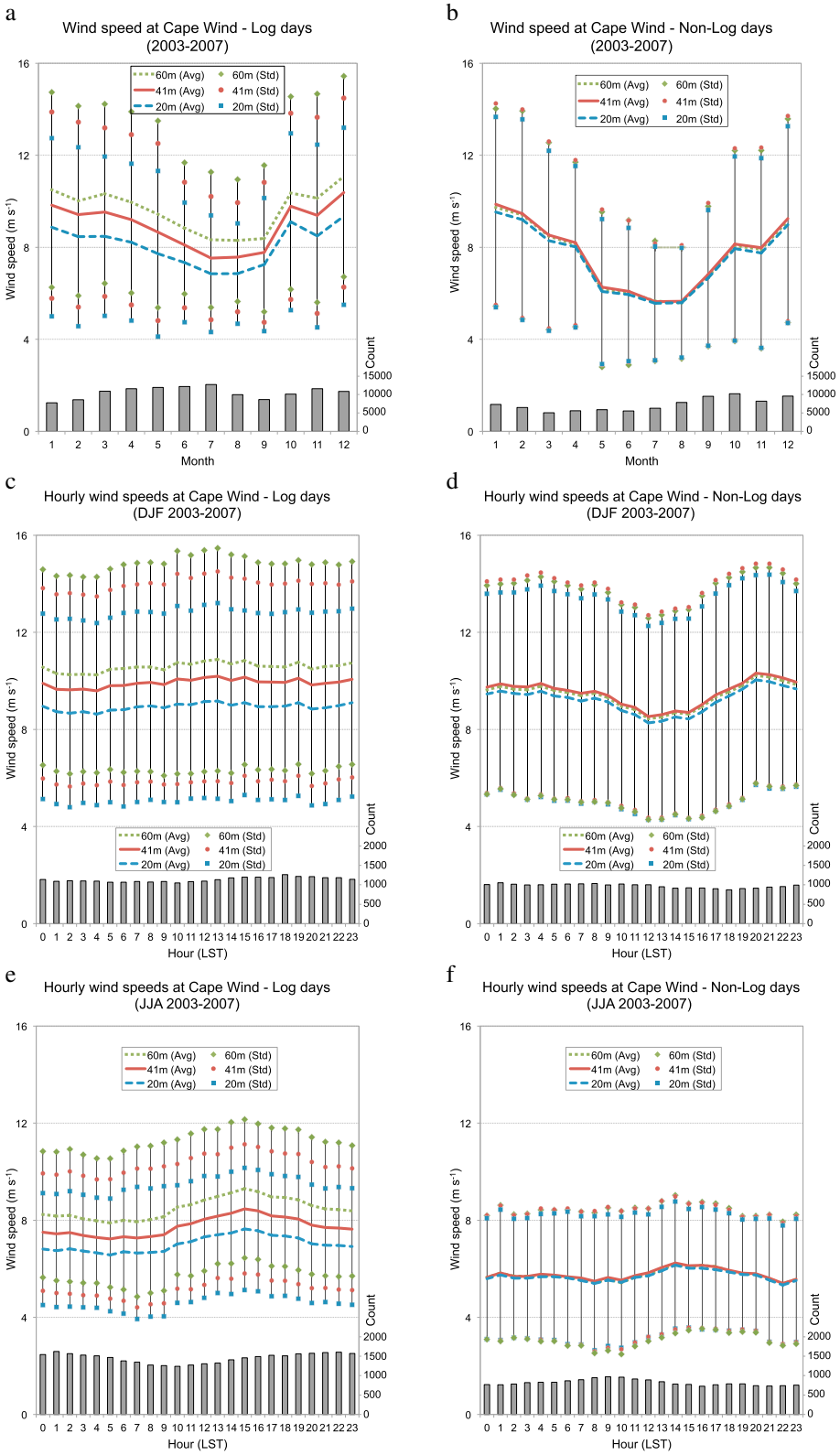

Figure 6. Distributions of wind speed at the three levels of the Cape Wind meteorological tower (20, 41, and 60 m AMSL) in 2003–2007 during (a, c, and e) log cases and (b, d, and f) nonlog cases: by month (Figures 6a and 6b), by hour in winter (Figures 6c and 6d), and by hour in summer (Figures 6e and 6f). The means (Avg) are represented with solid lines, the standard deviations (Std) with different markers for each level, and the count of valid 10 min records with grey column bars.

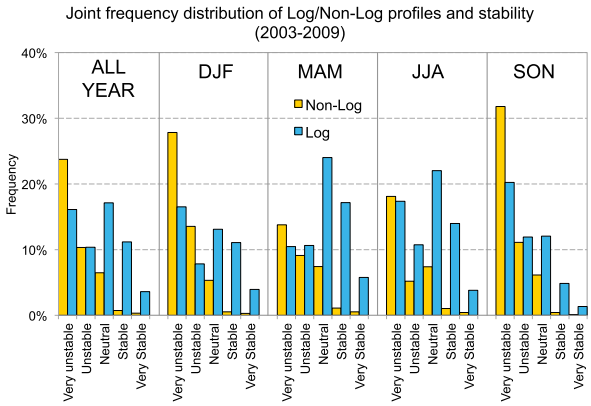

Figure 7. Joint frequency distribution of atmospheric stability categories and log/nonlog wind speed profiles at Cape Wind during 2003–2009 as a function of season.

that the common assumption of a logarithmic profile should be used with caution in the marine environment around CW. Monthly averages of both cases (Figures 6a and 6b) show that when the wind speed profile is nonlog, all three levels experience very similar mean wind speeds and standard deviations. This lack of wind shear is consistent with unstable conditions. Nonlog profiles are more common than log profiles in September and October, consistent with the predominance of unstable conditions in fall discussed previously. Nonlog cases are generally less windy than log cases, especially in the summer (Figures 6c–6f). This finding is consistent with *Wharton and Lundquist* [2012a, 2012b], who found that the weakest winds in a year occur during unstable conditions in summer and spring over land.

To verify that nonlog profiles are associated with unstable conditions, the Obukhov length analysis from section 3.1 is combined with the statistics on log versus nonlog profiles just discussed. For each season, the frequency distribution of very stable to very unstable conditions for log and nonlog days (Figure 7) indicates that nonlog profiles are significantly more common during unstable conditions than log cases, especially in SON and DJF. More importantly, nonlog profiles are very rare during stable and very stable conditions. As mentioned earlier, unstable conditions may also occur with log profiles, but stable conditions are hardly ever accompanied by nonlog profiles. The only exception is low-level jets with cores below 60 m, which occur only during stable conditions and yet would cause the vertical profile to become nonmonotonic. Such low-level jets are infrequent in Nantucket Sound [*Helmis et al*., 2013; *Mahrt et al*., 2014] and would explain the few percent cases that are stable or very stable and yet are classified as nonlog in Figure 7.

4.3. High TKE Under All Stabilities

Lastly, observations of TKE are presented from the three sources used previously, i.e., the historical and the IMPOWR data sets at the CW platform and the IMPOWR flights. Contrarily to *Wharton and Lundquist* [2012a, 2012b], who introduced thresholds of TKE for the various stability categories for inland locations, no such ranges can be identified offshore at CW in either the historical (Figure 8a) or the IMPOWR data sets (Figure 8b). While it is generally true that, for a given wind speed, TKE is higher during unstable than during stable conditions, values of TKE above a given threshold, like the $1\,m^2\,s^{-2}$ proposed threshold for unstable conditions over land [*Wharton and Lundquist*, 2012a, 2012b], can actually occur during stable conditions. Vice versa, values of TKE lower than $0.4\,m^2\,s^{-2}$, a previously proposed threshold for very stable conditions over land [*Wharton and Lundquist*, 2012a, 2012b], can occur during unstable conditions. For wind speeds greater than $11\,m\,s^{-1}$, very stable conditions may at times be characterized by higher TKE than unstable-to-neutral conditions, consistent with shear generation of TKE. From Figure 8, the clearest relationship is that TKE increases with wind speed offshore, as found previously [*Christakos et al*., 2013], in an nearly logarithmic fashion (see straight alignment of the dots in Figure 8). Similar conclusions can be reached from the IMPOWR sonic anemometer data, which were taken at lower heights (10 m for IMPOWR versus 20 m for the CW historical data set) and for more intermittent time periods, as described in section 2.2. This analysis suggests that ranges of TKE alone should not be used in the marine environment to characterize stability because TKE depends more strongly on wind speed than on atmospheric stability. However, combining wind shear profile and TKE analyses, both of which can be defined as qualitative methods, is effective because the results are consistent.

During the IMPOWR flights, high TKE values were recorded frequently (Table 2 and Figure 8b). Half of the flights revealed TKE in excess of $1\,m^2\,s^{-2}$, the threshold for unstable conditions discussed above. The other flights were conducted in late spring and showed TKE values that were lower than those observed in

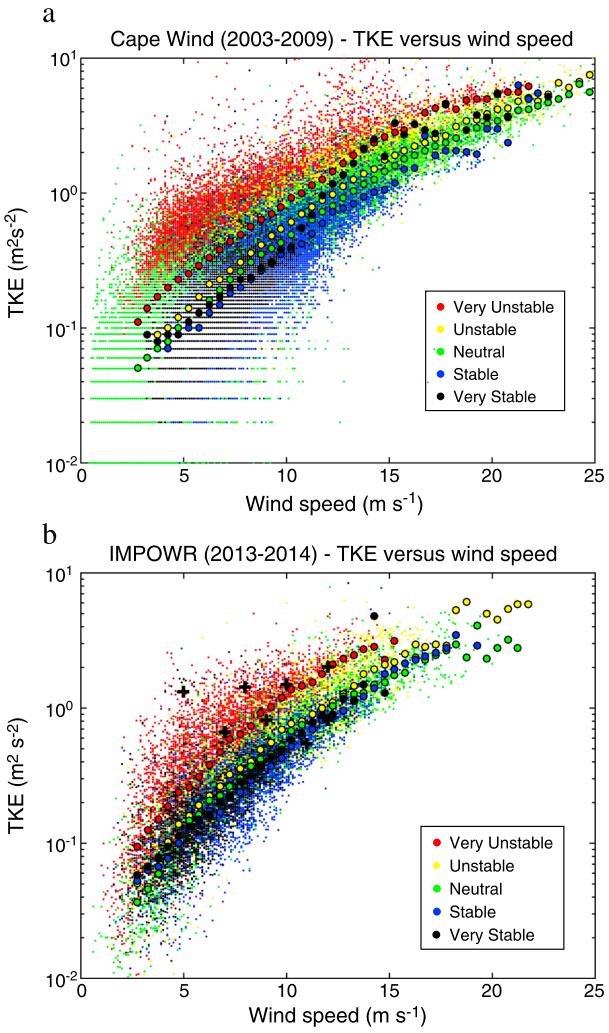

Figure 8. Observed TKE as a function of wind speed and stability at the Cape Wind platform: (a) from the 20 m sonic anemometer during 2003–2009 and (b) from the 10 m sonic anemometers during IMPOWR (2013–2014). The median TKE for each 0.5 m s^{-1} bin of wind speed is shown in large filled circles. The cross symbols represent the values recorded during the IMPOWR flights in Table 1. The bands in Figure 8b are caused by the data resolution of 10^{-2} m^2 s^{-2}.

summer, consistent with the higher frequency of neutral and stable conditions in spring shown in Figure 7. Note the lack of correlation between TKE and wind speed in the IMPOWR flights, possibly caused by the relatively long averaging time. Out of eight flights, five were conducted in southwesterly winds, which are associated with the highest frequency of stable conditions at CW (Figures 4b–4d), and yet TKE was often high. This confirms the previous findings that TKE is not clearly associated with stability offshore and that high TKE can be observed in stable conditions.

5. Conclusions

The most important finding of this study is that unstable conditions dominate in the marine boundary layer around the Cape Wind platform in Nantucket Sound. This is consistent with the average temperature difference between air and water being negative at buoy 44020 (by −1.07°C on average); thus, the ocean surface is generally warmer than the air, which is conducive to statically unstable conditions. In addition, turbulence is often high, even on stable days, although it depends primarily on wind speed; thus, mechanical mixing is high, either from interaction with surrounding land areas and their roughness or possibly due to the so-called wave pumping.

The second conclusion is that nonlog profiles, which are nonmonotonic profiles of wind speed with height (e.g., no shear, zigzags, local maxima/minima, or even negative shear), are common in unstable conditions and extremely rare in stable conditions and are a qualitative proxy for unstable conditions (or, more accurately, a proxy for nonstable conditions). On the other hand, TKE alone is not a valid proxy for atmospheric stability offshore because high TKE can be associated with stable conditions and low TKE with neutral or unstable conditions.

Third, southwesterly flows in spring and summer are nearly the only cases that are frequently characterized by stable conditions, which may explain the common occurrences of low-level jets (not shown here), which require stable conditions for formation.

Using different types of measurements (i.e., in situ measurements conducted on the Cape Wind platform and numerous flights during IMPOWR) and different types of analyses (from the more theoretical Obukhov length to the more qualitative wind speed profile analysis), as was done in this study, is a reliable approach to characterize stability conditions, because qualitative consistency of the results was found. Future work related to IMPOWR will focus on lidar measurements taken at Block Island and on numerical modeling efforts to improve existing boundary layer parameterizations in the offshore environment, given the unexpected predominance of unstable conditions identified here.

Acknowledgments
The authors thank Mark Rodgers of Cape Wind and Jack Arruda and Boone Davis of EMI Energy for providing the historical data collected at the Cape Wind platform and the much needed accompanying information. This research was funded by the U.S. Department of Energy (DE-EE0005377). The data collected during the IMPOWR campaign are available by request on the Data Archive and Portal (DAP) of the Department of Energy at https://a2e.pnnl.gov/study. The historical data set can be made available to other researchers, and the authors (impowr@geog.udel.edu) will facilitate permission to access the data.

References

Antoniou, I., S. M. Pedersen, and P. B. Enevoldsen (2010), Wind shear and uncertainties in power curve measurement and wind resources, *Wind Eng.*, *33*(5), 449–468, doi:10.1260/030952409790291208.

Archer, C. L., and M. Z. Jacobson (2003), Spatial and temporal distributions of U.S. winds and wind power at 80 m derived from measurements, *J. Geophys. Res.*, *108*(D9), 4289, doi:10.1029/2002JD002076.

Archer, C. L., and M. Z. Jacobson (2005), Evaluation of global wind power, *J. Geophys. Res.*, *110*, D12110, doi:10.1029/2004JD005462.

Arya, S. P. (1988), *Introduction to Micrometeorology*, 303 pp., Academic Press, San Diego, Calif.

Arya, S. P. (1999), *Air Pollution Meteorology and Dispersion*, 310 pp., Oxford Univ. Press, New York.

Banta, R. M., Y. L. Pichugina, N. D. Kelley, B. Jonkman, and W. A. Brewer (2008), Doppler lidar measurements of the Great Plains low-level jet: Applications to wind energy, *IOP Conf. Ser. Earth Environ. Sci.*, *1*, 012,020–012,025, doi:10.1088/1755-1307/1/1/012020.

Barthelmie, R., O. F. Hansen, K. Enevoldsen, J. Højstrup, S. Frandsen, S. Pryor, S. Larsen, M. Motta, and P. Sanderhoff (2005), Ten years of meteorological measurements for offshore wind farms, *J. Sol. Energy Eng.*, *127*(2), 170–176, doi:10.1115/1.1850489.

Barthelmie, R. J. (1999), The effects of atmospheric stability on coastal wind climates, *Meteorol. Appl.*, *6*(1), 39–47.

Bond, N. A., C. F. Dierking, and J. D. Doyle (2010), Research aircraft and wind profiler observations in Gastineau Channel during a Taku wind event, *Weather Forecasting*, *21*(4), 489–501, doi:10.1175/WAF932.1.

Brower, M. (2012), *Wind Resource Assessment: A Practical Guide to Developing a Wind Project*, 280 pp., John Wiley, Hoboken, N. J.

Christakos, K., J. Reuder, and B. R. Furevik (2013), Experimental characterization of the marine atmospheric boundary layer in the Havsul area, Norway, *Energy Procedia*, *35*, 121–127, doi:10.1016/j.egypro.2013.07.165.

Colle, B. A., M. J. Sienkiewicz, C. L. Archer, D. E. Veron, F. Veron, and W. Kempton (2016), Improving the mapping and prediction of offshore wind resources (IMPOWR): Experimental overview and first results, *Bull. Am. Meteorol. Soc.*, doi:10.1175/BAMS-D-14-00253.1.

Edson, J., et al. (2007), The coupled boundary layers and air–sea transfer experiment in low winds, *Bull. Am. Meteorol. Soc.*, *88*(3), 341–356, doi:10.1175/BAMS-88-3-341.

Eggers, A. J., R. Digumarthi, and K. Chaney (2003), Wind shear and turbulence effects on rotor fatigue and loads control, *J. Sol. Energy Eng.*, *125*, 402–409.

Emeis, S. (2013), *Wind Energy Meteorology*, 196 pp., Springer, New York.

Foken, T., M. Göckede, M. Mauder, L. Mahrt, B. D. Amiro, and J. W. Munger (2004), Post-field data quality control, in *Handbook of Micrometeorology: A Guide for Surface Flux Measurement and Analysis*, pp. 181–208, Kluwer, Dordrecht.

Goring, D. G., and V. I. Nikora (2002), Despiking acoustic Doppler velocimeter data, *J. Hydraul. Eng.*, *1281*, 117–126.

Gryning, S.-E., E. Batchvarova, B. Brümmer, H. Jørgensen, and S. Larsen (2007), On the extension of the wind profile over homogeneous terrain beyond the surface boundary layer, *Boundary Layer Meteorol.*, *124*(2), 251–268, doi:10.1007/s10546-007-9166-9.

Guo, Y., J. Keller, and W. LaCava (2015), Planetary gear load sharing of wind turbine drivetrains subjected to non-torque loads, *Wind Energy*, *18*(4), 757–768, doi:10.1002/we.1731.

Hansen, K. S., R. J. Barthelmie, L. E. Jensen, and A. Sommers (2012), The impact of turbulence intensity and atmospheric stability on power deficits due to wind turbine wakes at Horns Rev wind farm, *Wind Energy*, *15*, 183–196, doi:10.1002/we.512.

Hara, T., and P. P. Sullivan (2015), Wave boundary layer turbulence over surface waters in a strongly forced condition, *J. Phys. Oceanogr.*, *45*, 868–883.

Helmis, C. G., Q. Wang, G. Sgouros, S. Wang, and C. Halios (2013), Investigating the summertime low-level jet over the East Coast of the U.S.A.: A case study, *Boundary Layer Meteorol.*, *149*, 259–276, doi:10.1007/s10546-013-9841-y.

Helmis, C. G., G. Sgouros, and Q. Wang (2015), On the vertical structure and spectral characteristics of the marine low-level jet, *Atmos. Res.*, *152*, 74–81, doi:10.1016/j.atmosres.2013.11.005.

Högström, U. (1988), Non-dimensional wind and temperature profiles in the atmospheric surface layer: A re-evaluation, *Boundary Layer Meteorol.*, *42*(1–2), 55–78, doi:10.1007/BF00119875.

International Electrotechnical Commission (2009), *IEC 61400-3: Wind Turbines—Part 3. Design Requirements for Offshore Wind Turbines*, International Electrotechnical Commission, Geneva.

Jacobson, M. Z. (2005), *Fundamentals of Atmospheric Modeling*, 2nd ed., 813 pp., Cambridge Univ. Press, New York.

Kaimal, J. C., and J. E. Gaynor (1991), Another look at sonic thermometry, *Boundary Layer Meteorol.*, *56*, 401–410.

Kettle, A. J. (2014), Unexpected vertical wind speed profiles in the boundary layer over the southern North Sea, *J. Wind Eng. Ind. Aerodyn.*, *134*, 149–162, doi:10.1016/j.jweia.2014.07.012.

Lange, B., S. Larsen, J. Højstrup, and R. Barthelmie (2004), Importance of thermal effects and sea surface roughness for offshore wind resource assessment, *J. Wind Eng. Ind. Aerodyn.*, *92*(11), 959–988, doi:10.1016/j.jweia.2004.05.005.

Mahrt, L., D. Vickers, and E. L. Andreas (2014), Low-level wind maxima and structure of the stably stratified boundary layer in the coastal zone, *J. Appl. Meteorol. Climatol.*, *53*, 363–376, doi:10.1175/JAMC-D-13-0170.1.

Metzger, M., B. J. McKeon, and H. Holmes (2007), The near-neutral atmospheric surface layer: Turbulence and non-stationarity, *Philos. Trans. R. Soc. A*, *365*(1852), 859–876, doi:10.1098/rsta.2006.1946.

Mironov, D. V., and P. P. Sullivan (2015), Second-moment budgets and mixing intensity in the stably stratified atmospheric boundary layer over thermally heterogeneous surfaces, *J. Atmos. Sci.*, doi:10.1175/JAS-D-15-0075.1, in press.

Motta, M., R. J. Barthelmie, and P. Vølund (2005), The influence of non-logarithmic wind speed profiles on potential power output at Danish offshore sites, *Wind Energy*, *8*(2), 219–236, doi:10.1002/we.146.

Nunalee, C. G., and S. Basu (2013), Mesoscale modeling of coastal low-level jets: Implications for offshore wind resource estimation, *Wind Energy*, *17*(8), 1199–1216, doi:10.1002/we.1628.

Obukhov, A. M. (1946), Turbulentnost' v temperaturnoj – neodnorodnoj atmosfere (Turbulence in an atmosphere with a non-uniform temperature), *Trudy Inst. Theor. Geofiz. AN SSSR*, *1*, 95–115.

Panofsky, H. A., H. Tennekes, D. H. Lenschow, and J. C. Wyngaard (1977), The characteristics of turbulent velocity components in the surface layer under convective conditions, *Boundary Layer Meteorol.*, *11*, 355–361.

Pichugina, Y. L., R. M. Banta, W. A. Brewer, S. P. Sandberg, and R. M. Hardesty (2012), Doppler lidar-based wind-profile measurement system for offshore wind-energy and other marine boundary layer applications, *J. Appl. Meteorol. Climatol.*, *51*, 327–349.

Rajewski, D. A., et al. (2013), Crop Wind Energy Experiment (CWEX): Observations of surface-layer, boundary layer, and mesoscale interactions with a wind farm, *Bull. Am. Meteorol. Soc.*, *94*(5), 655–672, doi:10.1175/BAMS-D-11-00240.1.

Sathe, A., S.-E. Gryning, and A. Pena (2011), Comparison of the atmospheric stability and wind profiles at two wind farm sites over a long marine fetch in the North Sea, *Wind Energy*, *14*(6), 767–780, doi:10.1002/we.456.

Schotanus, P., F. T. M. Nieuwstadt, and H. A. R. De Bruin (1983), Temperature measurement with a sonic anemometer and its application to heat and moisture fluxes, *Boundary Layer Meteorol.*, *26*, 81–93.

Stull, R. B. (1988), *An Introduction to Boundary Layer Meteorology*, 666 pp., Kluwer Acad., Norwell, Mass.

Sullivan, P. P., J. C. McWilliams, and E. G. Patton (2014), Large-eddy simulation of marine atmospheric boundary layers above a spectrum of moving waves, *J. Atmos. Sci.*, *71*(11), 4001–4027, doi:10.1175/JAS-D-14-0095.1.

Sumner, J., and C. Masson (2006), Influence of atmospheric stability on wind turbine power performance curves, *J. Sol. Energy Eng.*, *128*(4), 531–538, doi:10.1115/1.2347714.

van den Berg, G. P. (2008), Wind turbine power and sound in relation to atmospheric stability, *Wind Energy*, *11*(2), 151–169, doi:10.1002/we.240.

Van Wijk, A. J. M., A. C. M. Beljaars, A. A. M. Holtslag, and W. C. Turkenburg (1990), Evaluation of stability corrections in wind speed profiles over the North Sea, *J. Wind Eng. Ind. Aerodyn.*, *33*(3), 551–566, doi:10.1016/0167-6105(90)90007-Y.

Vanderwende, B. J., and J. K. Lundquist (2012), The modification of wind turbine performance by statistically distinct atmospheric regimes, *Environ. Res. Lett.*, *7*(3), 7, doi:10.1088/1748-9326/7/3/034035.

Vecenaj, Z., D. Belusic, V. Grubisic, and B. Grisogono (2012), Along-coast features of Bora-related turbulence, *Boundary Layer Meteorol.*, *143*, 527–545.

Wagner, R., I. Antoniou, S. M. Pedersen, M. S. Courtney, and H. E. Jørgensen (2009), The influence of the wind speed profile on wind turbine performance measurements, *Wind Energy*, *12*, 348–362, doi:10.1002/we.297.

Wharton, S., and J. K. Lundquist (2012a), Assessing atmospheric stability and its impacts on rotor-disk wind characteristics at an onshore wind farm, *Wind Energy*, *15*(4), 525–546, doi:10.1002/we.483.

Wharton, S., and J. K. Lundquist (2012b), Atmospheric stability affects wind turbine power collection, *Environ. Res. Lett.*, *7*(1), 014005, doi:10.1088/1748-9326/7/1/014005.

Wilczak, J. M., S. P. Oncley, and S. A. Stage (2001), Sonic anemometer tilt correction algorithms, *Boundary Layer Meteorol.*, *99*, 127–150.

Wyngaard, J. C. (2010), *Turbulence in the Atmosphere*, 218 pp., Cambridge Univ. Press, New York.

Zhang, J. A., F. D. Marks, M. T. Montgomery, and S. Lorsolo (2011), An estimation of turbulent characteristics in the low-level region of intense hurricanes Allen (1980) and Hugo (1989), *Mon. Weather Rev.*, *139*(5), 1447–1462, doi:10.1175/2010MWR3435.1.